Journal of Information Systems Engineering and Management
2025, 10(4)
e-ISSN: 2468-4376
https://www.jisem-journal.com/

Research Article

Design of Advanced Passivity-Fuzzy Logic Controller Compared to Control Techniques for Doubly-Fed Induction Generator in Wind Energy Conversion System

Allali Izzeddine[1,*], Abdelber Bendaoud [2], Boubekeur Dehiba [1]
[1] *IRECOM Laboratory, Faculty of Electrical Engineering, Djilali Liabès University of Sidi Bel-Abbès, Algeria.*
[2] *APELEC Laboratory, Faculty of Electrical Engineering, Djilali Liabès University of Sidi Bel-Abbès, Algeria.*
* *Corresponding Author:* izzeddine.allali@univ-sba.dz

ARTICLE INFO

Received: 10 Jul 2025
Revised: 02 Aug 2025
Accepted: 24 Aug 2025

ABSTRACT

This paper presents a new passivity-fuzzy logic control strategy for a doubly-fed induction generator (DFIG) within a wind energy conversion system (WECS). The strategy addresses the high uncertainty of complex nonlinear systems by combining interconnection and damping assignment (IDA) passivity-based control (PBC) with interval type-2 fuzzy logic control (IT2-FLC). IDA-PBC compensates for nonlinearities without eliminating them, and IT2-FLC enhances uncertainty handling by managing vagueness and unreliable data. The proposed method effectively regulates the flow of active and reactive power to the grid, adapts to varying generator parameters, and achieves accurate reference tracking, thereby ensuring stable operation. A comprehensive comparative analysis of four controllers is presented, evaluating their performance under varying wind speeds (WS) and parameter uncertainties. Performance is assessed using criteria such as response time, reference tracking, power ripple, time-integrated error metrics, and robustness. The findings show that the suggested passivity-fuzzy logic control method outperforms other advanced methods.

Keywords: Doubly fed induction generator; IDA-PBC control; Interval type-2 fuzzy logic control; Passivity-fuzzy logic control; Comparative study.

INTRODUCTION

Wind energy is a competitive alternative to other renewable energy sources. Its recent rapid expansion is due to its significant contribution to reducing emissions from conventional thermal power stations, as well as the decreasing availability of fuels and rising energy production costs using traditional methods. Additionally, concerns about the environmental impact of thermal and nuclear power generation are becoming increasingly prominent in public opinion. Wind power systems are among the most advanced and well-established solutions for harnessing wind energy [1, 2]. Globally, the capacity of new wind power installations reached a record 117 GW by the end of 2024, raising the total cumulative capacity to 1,136 GW [3].

The most recent generation of wind turbines (WT) functions at variable speeds, enhancing energy efficiency, minimizing mechanical stress, and improving the quality of the generated electrical power. Unlike fixed-speed wind turbines, these systems employ control algorithms to regulate both active and reactive power (Ps and Qs) production dynamically at any given moment.

A large share of modern wind turbines use DFIGs due to advantages like easy operation, variable speed capability (up to 30% of synchronous speed), low maintenance, affordability, improved power quality, and durability. Their rotor voltage is controlled by two inverters, enabling precise power regulation that makes DFIGs among the most reliable solutions for managing variable wind speeds [4, 5].

To regulate a doubly fed induction machine (DFIM) system, classical control techniques must be employed, incorporating proportional, integral, and derivative actions. To successfully construct the system, it is necessary to understand all of its parameters and respond appropriately. However, mistakes and incorrect information are widespread, and the fact that system variables are linked makes vector control (VC) more difficult [6, 7]. Nonlinear techniques like sliding mode control (SMC) offer a solution, effectively managing parameter variations, disturbances, and unmodeled dynamics in both linear and nonlinear systems [8, 9]. The biggest problem with this method is that it

Journal of Information Systems Engineering and Management
2025, 10(4)
e-ISSN: 2468-4376
https://www.jisem-journal.com/

Research Article

causes the system to switch more often since control switching happens when the system state crosses the sliding surface. This can result in system chattering. This may cause high-frequency unmodeled modes, which might hurt the nonlinear control system [10].

Passivity -based control (PBC) is a proven and effective approach for designing robust control systems in physical applications. Rooted in established physical principles, it is widely applied in electrical, mechanical, and electromechanical system management. PBC's key advantage is that it attenuates rather than suppresses nonlinearities, reorganizing the system's natural energy and integrating control elements to meet objectives. This method enhances robustness and ensures smooth controller calculations by eliminating nonlinear discontinuities [11].

Fuzzy logic is a mathematical method capable of emulating human reasoning by processing imprecise data, leading to conclusions despite vague information. These systems are subject to uncertainties due to variations in linguistic terms and noise in the measured data.

Uncertainties induce uncertain membership functions (MF).Type-1 fuzzy sets feature exact, two-dimensional membership functions but are insufficient for managing such uncertainties. To overcome this limitation, Zadeh proposed type-2 fuzzy sets, wherein the membership degree itself is represented as a fuzzy set within the interval [0, 1]. As a result, a type-2 fuzzy set is three-dimensional. The third dimension provides an additional degree of freedom for taking linguistic uncertainties into account, particularly when the form or parameters of the MF are uncertain [12].

The passivity-Fuzzy Logic Controller (PFLC) represents an innovative control methodology that IDA-PBC with IT2-FLC. This facilitates enhanced management of nonlinearities. The IDA-PBC control strategy is designed for systems with Port-Controlled Hamiltonian (PCH) models, which incorporate interconnection assignment and damping injection. Grounded in energy shaping and passivation principles, this method incorporates a damping factor that systematically addresses nonlinear terms while optimizing interconnects and damping structures [13]. Integrating Type 2 Fuzzy Logic into the controller improves the quality of both Ps and Qs. This results in superior performance regarding reference tracking, disturbance resistance, and robustness against parameter variations in a doubly-fed induction generator.

This paper provides a thorough comparative analysis of VC, SMC, IDA-PBC, and PFLC controllers for a DFIG-based WECS. It includes theoretical analysis, modeling, and simulations, developing active and reactive power control strategies to optimize power output. Thus, we examined and compared the performance of the four control strategies using reference tracking and robustness criteria.

Conversion of Wind Energy

Figure 1 illustrates a WECS where the operation of a WT encompasses multiple disciplines, including aerodynamics, mechanics, electricity, and automation.

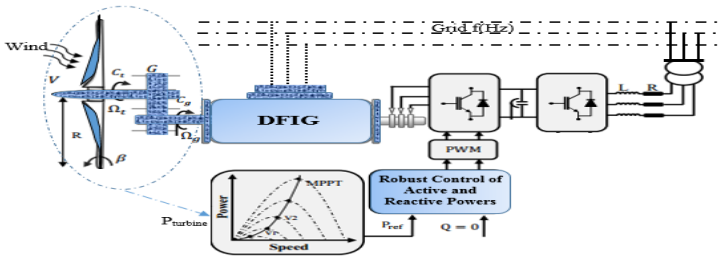

Fig. 1. Principle of energy conversion.

Modeling the Turbine

Since the WT can only recover a fraction of the wind's power, the aerodynamic power appearing at the turbine rotor is written as [14]:

$$P_m = \frac{1}{2}\rho\pi R^2 v^3 C_p(\lambda,\beta) \quad (1)$$

Where ρ denotes the air density (1.225 kg/m³) and R represents the radius of the turbine blade, Cp(λ) is the power coefficient. This coefficient varies according to the specific design characteristics of the turbine. The tip speed ratio, λ, is expressed as follows:

$$\lambda = \frac{\Omega.R}{v} \quad (2)$$

Journal of Information Systems Engineering and Management
2025, 10(4)
e-ISSN: 2468-4376
https://www.jisem-journal.com/

Research Article

Ω represents the rotational speed of the turbine rotor. The theoretical maximum Cp is 0.593 [15]. The input torque is given by [14, 16]:

$$T_m = \frac{P_m}{\Omega} = \frac{1}{2\lambda}\rho\pi R^3 v^2 C_p(\lambda,\beta) \quad (3)$$

Equation (4) gives the value of Cp for the wind turbine system [17, 18]. Cp, which is related to the output power, is at its maximum when the tilt angle is 0°.

$$C_p(\lambda,\beta) = \left(0.5 - 0.00167(\beta - 2)\right)\sin\left[\frac{\pi(\lambda+0.1)}{18.5-0.3(\beta-2)}\right] - 0.00184(\lambda-3)(\beta-2) \quad (4)$$

To enhance WT performance, the maximum power point tracking (MPPT) control system should regulate the speed while maintaining the β value at its minimum level. This maximises the Cp at the λ_{opt}, thereby achieving the maximum power coefficient ($C_{p\text{-}max}$) [9, 19]. The torque reference T_{m-ref} was formulated by [20, 21]:

$$T_{m-ref} = \frac{\rho}{2}\frac{c_{p-max}}{\lambda_{opt}^3}\pi\frac{R_t^5}{G}\Omega_{mec}^2 \quad (5)$$

The pitch controller keeps an eye on the turbine's power production and changes the pitch of the blades to get the best performance in different wind situations. This keeps the wind speed from becoming too high. This keeps the turbine construction safe by limiting the maximum rotation speed and keeping the wind turbine system's energy production at its normal, steady level [19, 21].

Modeling of the DFIG

The formulations of the stator and rotor voltages along the d, q axis are expressly provided by [19]:

$$\begin{cases} V_{sd} = R_s I_{sd} + \frac{d\phi_{sd}}{dt} - \omega_s\phi_{sq} \\ V_{sq} = R_s I_{sq} + \frac{d\phi_{sq}}{dt} + (\omega_s - \omega_r)\phi_{sd} \\ V_{rd} = R_r I_{rd} + \frac{d\phi_{rd}}{dt} - \omega_s\phi_{rq} \\ V_{rq} = R_r I_{rq} + \frac{d\phi_{rq}}{dt} + (\omega_s - \omega_r)\phi_{rd} \end{cases} \quad (6)$$

The rotor and stator fluxes are represented as follows.

$$\begin{cases} \phi_{sd} = L_s I_{sd} + M I_{rd} \\ \phi_{sq} = L_s I_{sq} + M I_{rq} \\ \phi_{rd} = L_r I_{rd} + M I_{sd} \\ \phi_{rq} = L_r I_{rq} + M I_{sq} \end{cases} \quad (7)$$

The system's mechanical equation is as follows:

$$\Gamma_{em} = \Gamma_r + C_f\Omega_{mec} + J_T\frac{d\Omega_{mec}}{dt} \quad (8)$$

Torque is defined as follows:

$$\Gamma_{em} = p\frac{M}{L_s}(\phi_{sd}I_{rq} - \phi_{sq}I_{rd}) \quad (9)$$

Design of the Vector Controller

We align the stator flux with a rotating reference frame to enable DFIG control, allowing us to manage active and reactive power separately. For medium- and high-power wind turbines, stator resistance (Rs) is relatively low. Consequently, the DFIG electrical equations are as follows [22]:

$$\Phi_{sd} = \phi_s \quad et \quad \phi_{sq} = 0 \quad (10)$$

The flow equation (7) can be expressed as follows:

$$\begin{cases} \phi_{sd} = L_s I_{sd} + M I_{rd} \\ 0 = L_s I_{sq} + M I_{rq} \end{cases} \quad (11)$$

The stator voltage equations may be expressed in a simplified form as follows:

$$V_{sd} = 0, \quad V_{sq} = V_s = \omega_s\phi_s \quad (12)$$

The rotor voltages V_{rd} and V_{rq} regulate the stator power, enabling the independent management of reactive and active power. In the d-q reference frame, the power can be represented as:

Journal of Information Systems Engineering and Management
2025, 10(4)
e-ISSN: 2468-4376
https://www.jisem-journal.com/

Research Article

$$\begin{cases} P_s = V_{sd}I_{sd} + V_{sq}I_{sq} = -V_s\frac{M}{L_s}I_{rq} \\ Q_s = V_{sq}I_{sd} - V_{sd}I_{sq} = -V_s\frac{M}{L_s}I_{rd} + V_s\frac{\phi_s}{L_s} \end{cases} \quad (13)$$

$$\begin{cases} V_{rd} = R_rI_{rd} + \left(L_r - \frac{M^2}{L_s}\right)\frac{dI_{rd}}{dt} - g\omega_s\left(L_r - \frac{M^2}{L_s}\right)I_{rq} \\ V_{rq} = R_rI_{rq} + \left(L_r - \frac{M^2}{L_s}\right)\frac{dI_{rq}}{dt} + g\omega_s\left(L_r - \frac{M^2}{L_s}\right)I_{rd} + g\frac{MV_s}{L_s} \end{cases} \quad (14)$$

According to equation (14), the Ps of the stator depends solely on the Irq, while the Qs depends on the Ird. The decoupled control of the stator's Ps and Qs was performed in the stator flux reference frame using indirect stator power vector control, as illustrated in Figure 2.

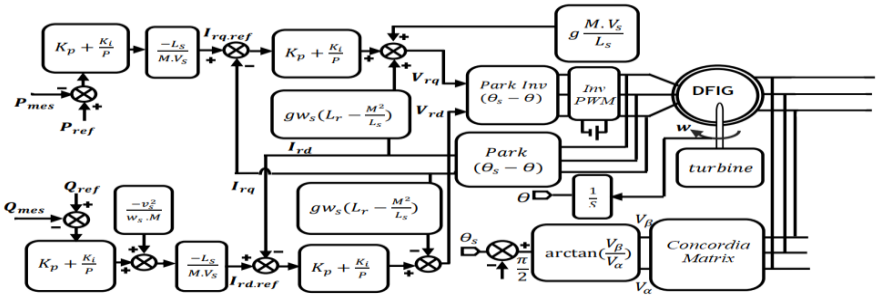

Fig. 2. Diagram of the vector control structure.

Design of the Sliding Mode Controller

SMC is a control technology prized for its simplicity and robustness. Studied for over 60 years, it has numerous applications [23]. SMC entails first mapping the system's states inside a meticulously selected area, followed by the formulation of a control rule that guarantees the system's continual presence within this region [24].

Power control

To control power, we choose n=1. The expression for the Ps and Qs control surface is simplified to:

$$\begin{cases} s(P_s) = (P_s^{ref} - P_s) \\ s(Q_s) = (Q_s^{ref} - Q_s) \end{cases} \quad (15)$$

A surface's derivative is:

$$\begin{cases} \dot{s}(\mathrm{P_s}) = (\dot{P}_s^{ref} - \dot{P}_s) \\ \dot{s}(Q_s) = (\dot{Q}_s^{ref} - \dot{Q}_s) \end{cases} \quad (16)$$

The power expression (Equation 13) is substituted with

$$\begin{cases} \dot{s}(P_s) = (\dot{P}_s^{ref} + V_s\frac{M}{L_s}\dot{I}_{rq}) \\ \dot{s}(Q_s) = \dot{Q}_s^{ref} - \left(-V_s\frac{M}{L_s}\dot{I}_{rd}\right) \end{cases} \quad (17)$$

Equation (14) is utilized to derive the current from the voltage equation.

$$\begin{cases} \dot{s}(P_S) = \dot{P}_s^{ref} + V_s\frac{M}{\sigma.L_r.L_s}(V_{rq} - R_rI_{rq} - \mathrm{g}\omega_s\sigma L_rI_{rd} - \mathrm{g}\frac{MV_s}{L_s}) \\ \dot{s}(Q_s) = \dot{Q}_s^{ref} + V_s\frac{M}{\sigma L_rL_s}(V_{rd} - R_rI_{rd} + \mathrm{g}\omega_s\sigma L_rI_{rq}) \end{cases} \quad (18)$$

The region attains attractiveness and invariance upon satisfaction of the convergence condition delineated by the Lyapunov equation.

$$S(X)\dot{S}(X) \leq 0 \quad (19)$$

In the system of equations (18), we replace V_{rd} and V_{rq} with $(V_{rd}^{eq} + V_{rd}^{n})$ and $(V_{rq}^{eq} + V_{rq}^{n})$, respectively, in accordance with the sliding mode theory:

$$\begin{cases} \dot{s}(P_S) = \dot{P}_s^{ref} + V_s\frac{M}{\sigma.L_r.L_s}((V_{rq}^{eq} + V_{rq}^{n}) - R_rI_{rq} - \mathrm{g}\omega_s\sigma L_rI_{rd} - \mathrm{g}\frac{MV_s}{L_s}) \\ \dot{s}(Q_s) = \dot{Q}_s^{ref} + V_s\frac{M}{\sigma L_rL_s}((V_{rd}^{eq} + V_{rd}^{n}) - R_rI_{rd} + \mathrm{g}\omega_s\sigma L_rI_{rq}) \end{cases} \quad (20)$$

Journal of Information Systems Engineering and Management
2025, 10(4)
e-ISSN: 2468-4376
https://www.jisem-journal.com/

Research Article

Where: $\sigma = 1 - (L_m^2/L_sL_r)$ denotes the leakage factor, and g represents the slip of the induction machine. In sliding mode and steady state, the following conditions apply:

$$\begin{cases} s(P_s) = 0, \dot{s}(P_s) = 0, V_{rq}^n = 0 \\ s(Q_s) = 0, \dot{s}(Q_s) = 0, V_{rd}^n = 0 \end{cases} \quad (21)$$

By substituting the system of equations (21) into (20), the formulas for the equivalent commands V_{qr}^{eq} and V_{rd}^{eq} can be expressed as follows:

$$\begin{cases} V_{rq}^{eq} = -\dot{P}_s^{ref} \frac{\sigma.L_r.L_s}{MV_s} + R_r I_{rq} + g\omega_s \sigma L_r I_{rd} + g\frac{MV_s}{L_s} \\ V_{rd}^{eq} = -\dot{Q}_s^{ref} \frac{\sigma.L_r.L_s}{MV_s} + R_r I_{rd} - g\omega_s \sigma L_r I_{rq} \end{cases} \quad (22)$$

So, the switching term may be written like this:

$$\begin{cases} V_{rq}^n = -K_{V_{rq}} \text{sign}(s(P_s)) \\ V_{rd}^n = -K_{V_{rd}} \text{sign}(s(Q_s)) \end{cases} \quad (23)$$

For the control system to remain stable, gains $K_{V_{rq}}$ and $K_{V_{rd}}$ must be positive.

Equations (22) and (23) make it possible to develop a block diagram for SMC when applied to a DIFG, as illustrated in Figure 3.

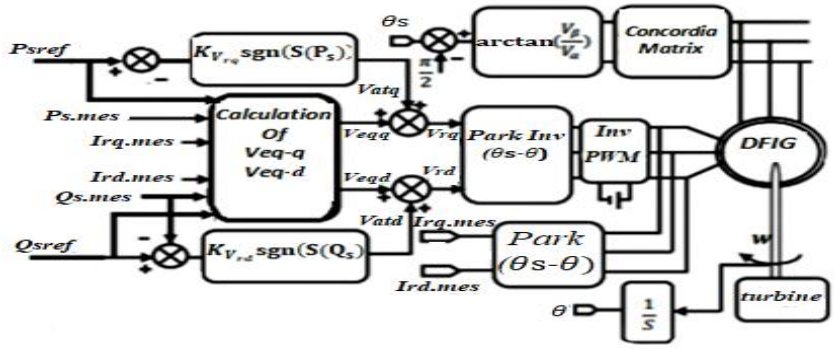

Fig. 3. Schematic diagram of the sliding mode control structure.

Design of the IDA-PBC

The fundamental concept of IDA-PBC is to modify the internal architecture to attain stability and the required equilibrium. Control by interconnection assignment and damping injection defines the closed-loop (CL) system by designating a target PCH, hence improving stability through damping injection [13].

Double-fed induction generator PCH structure

The initial phase of the IDA-PBC methodology involves systematically designing the PCH structure for DFIG based on the model in equation (6), from which the following equations are derived:

$$\begin{cases} \frac{d\phi_{sd}}{dt} = \boldsymbol{V_{sd} - R_s I_{sd} + \omega_s L_s I_{sq} + \omega_s M I_{rq}} \\ \frac{d\phi_{sq}}{dt} = \boldsymbol{V_{sq} - R_s I_{sq} - \omega_s L_s I_{sd} - \omega_s M I_{rd}} \\ \frac{d\phi_{rd}}{dt} = \boldsymbol{V_{rd} - R_r I_{rd} + (\omega_s - \omega_r) L_r I_{rq} + (\omega_s - \omega_r) M I_{sq}} \\ \frac{d\phi_{rq}}{dt} = \boldsymbol{V_{rq} - R_s I_{rq} - (\omega_s - \omega_r) L_r I_{rd} + (\omega_s - \omega_r) M I_{sd}} \end{cases} \quad (24)$$

The energy function can be written as follows:

$$H(x) = \frac{1}{2} x_e^T L^{-1} x_e + \frac{1}{2J_{DFIG}} x_m^2 \quad (25)$$

With: $L = \begin{bmatrix} L_s I_2 & MI_2 \\ MI_2 & L_r I_2 \end{bmatrix}, I_2 = \begin{bmatrix} 1 & 0 \\ 0 & 1 \end{bmatrix}$

It is provided in the following manner that the partial derivatives of energy with regard to the state variables are displayed:

$$\begin{cases} \frac{\partial H}{\partial x_e} = L^{-1} x_e \\ \frac{\partial H}{\partial x_m} = J^{-1} x_m \end{cases} \Rightarrow \begin{cases} \frac{\partial H}{\partial x_e} = I = [I_s^T I_r^T]^T \\ \frac{\partial H}{\partial x_m} = \omega \end{cases} \quad (26)$$

The matrices presented below correspond to the command, damping, and interconnection components:

Journal of Information Systems Engineering and Management
2025, 10(4)
e-ISSN: 2468-4376
https://www.jisem-journal.com/

Research Article

$$J(x)=\begin{bmatrix}-\omega_s L_s J_2 & -\omega_s M J_2 & 0_{2\times1}\\ -\omega_s L_s J_2 & -\omega_r L_s J_2 & M J_2 I_s\\ 0_{1\times2} & M I_S^T J_2 & 0\end{bmatrix}, R(x)=\begin{bmatrix}R_s I_2 & 0_{2\times2} & 0_{2\times1}\\ 0_{2\times2} & R_r I_2 & 0_{2\times1}\\ 0_{1\times2} & 0_{1\times2} & T_f\end{bmatrix} \quad (27)$$

$$g(x)=\begin{bmatrix}I_2 & 0_{2\times2} & 0_{2\times1}\\ 0_{2\times2} & I_2 & 0_{2\times1}\\ 0_{1\times2} & 0_{1\times2} & 1\end{bmatrix}, u=[V_s^T \quad V_r^T \quad T_r]^T \quad (28)$$

With:

$$0_{2\times2}=\begin{bmatrix}0 & 0\\ 0 & 0\end{bmatrix}, 0_{2\times1}=\begin{bmatrix}0\\ 0\end{bmatrix}, 0_{1\times2}=[0\ 0],\ J_2=\begin{bmatrix}0 & -1\\ 1 & 0\end{bmatrix}, V_s^T=\begin{bmatrix}V_{sd}\\ V_{sq}\end{bmatrix}\quad V_r^T=\begin{bmatrix}V_{rd}\\ V_{rq}\end{bmatrix}$$

$$J(x)=J(x)^{-1}, R(x)=R(x)^T \geq 0 \quad (29)$$

These matrices may be utilized to represent the PCH model:

$$\dot{x}=\left[\begin{bmatrix}-\omega_s L_s J_2 & -\omega_s M J_2 & 0_{2\times1}\\ -\omega_s M J_2 & -\omega_r L_s J_2 & M J_2 I_s\\ 0_{1\times2} & M I_S^T J_2 & 0\end{bmatrix}-\begin{bmatrix}R_s I_2 & 0_{2\times2} & 0_{2\times1}\\ 0_{2\times2} & R_r I_2 & 0_{2\times1}\\ 0_{1\times2} & 0_{1\times2} & T_f\end{bmatrix}\right]\nabla H+\begin{bmatrix}I_2 & 0_{2\times2} & 0_{2\times1}\\ 0_{2\times2} & I_2 & 0_{2\times1}\\ 0_{1\times2} & 0_{1\times2} & 1\end{bmatrix}\begin{bmatrix}V_s^T\\ V_r^T\\ T_r\end{bmatrix} \quad (30)$$

$$\dot{y}=\begin{bmatrix}I_2 & 0_{2\times2} & 0_{2\times1}\\ 0_{2\times2} & I_2 & 0_{2\times1}\\ 0_{1\times2} & 0_{1\times2} & 1\end{bmatrix}\nabla H \quad (31)$$

Calculation of the control voltages Vrd and Vrq

In order to calculate the control voltages, it is necessary to find $J_d(x)$ and $R_d(x)$. The CL system can be written as follows to obtain the controller's $J_d(x)$ and $R_d(x)$:

$$f(x)+g(x)u=\big(J_d(x)-R_d(x)\big)\partial H_d(x) \quad (32)$$

Where:

$$\begin{aligned}J_d(x)&=J(x)+J_a(x)\\ R_d(x)&=R(x)+R_a(x)\\ H_d(x)&=H(x)+H_a(x)\end{aligned} \quad (33)$$

$R_a(x)$, $J_a(x)$, and $H_a(x)$ denote, respectively, the interconnection matrix, the damping matrix, and the energy introduced by the controller.

According to equation (32), this may be represented as follows:

$$\big(J(x)+J_a(x)-R(x)\ +R_a(x)\big)\partial H_d(x)=-\big(J_a(x)-R_a(x)\big)\partial H(x)+g(x)u \quad (34)$$

Equation (34) is equivalent to:

$$\big(J_d(x)-R_d(x)\big)\partial H_a(x)=-\big(J_a(x)-R_a(x)\big)\partial H(x)+g(x)u \quad (35)$$

So, the desired total energy:

$$H_d(x)=\frac{1}{2}(x_e-x_e^*)^T L^{-1}(x_e-x_e^*)+\frac{1}{2J_{DFIG}}(x_m-x_m^*)^2 \quad (36)$$

So:

$$H_a(x)=H_d(x)-H(x)=-x_e^T L^{-1}x_e-\frac{1}{J_{DFIG}}x_m^* x_m+\frac{1}{2}x_e^{*T}L^{-1}x_e^*+\frac{1}{2J_{DFIG}}x_e^{*2} \quad (37)$$

With : $\partial H_a(x)=\begin{bmatrix}-I^*\\ -\omega^*\end{bmatrix}$, where $I=[I_{sd}I_{sq}I_{rd}I_{rq}]^T$

Using this relationship transforms (35) into:

$$\big(J_d(x)-R_d(x)\big)\begin{bmatrix}-I^*\\ -\omega^*\end{bmatrix}=-\big(J_a(x)-\ R_a(x)\big)\begin{bmatrix}I\\ \omega\end{bmatrix}+g(x)u \quad (38)$$

In (38), the command Vr appears on lines 3 and 4 of the matrix. As a result:

$$J_a(x)=\begin{bmatrix}0_{2\times2} & 0_{2\times2} & 0_{2\times1}\\ 0_{2\times2} & 0_{2\times2} & -J_{rm}(x)\\ 0_{1\times2} & J_{rm}^T(x) & 0\end{bmatrix}, R_a(x)=\begin{bmatrix}0_{2\times2} & 0_{2\times2} & 0_{2\times1}\\ 0_{2\times2} & rI_2 & 0_{2\times1}\\ 0_{1\times2} & 0_{1\times2} & 0\end{bmatrix} \quad (39)$$

Where:

$J_{rm}^T(x) \in \Re^{2\times1}$ to be determined.

Journal of Information Systems Engineering and Management
2025, 10(4)
e-ISSN: 2468-4376
https://www.jisem-journal.com/

Research Article

r: This is an extra resistance that is present. It relates to the currents. One of its applications is to dampen transitory fluctuation.
The matrices $J_a(x)$ and $R_a(x)$ are replaced, and the following is obtained using the formula (37):

$$J_{rm}^T(x) = M\frac{(I_r - I_r^*)^T}{|I_r - I_r^*|^2}(I_s - I_s^*)^T J_2 I_r^* \tag{40}$$

So:

$$V_r = V_r^* - (\omega - \omega^*)(L_r J_2 I_r^* + J_{rm}(x)) - M\omega^* J_2(I_s - I_s^*) - rI_2(I_r - I_r^*) \tag{41}$$

The order is, regrettably, singular regarding equilibrium. Adding a depreciation variable can effectively eliminate this singularity. We continue to retain $J_d(x)$ and $H_d(x)$ as previously established and modify the R_a matrix to the subsequent form:

$$R_a(x) = \begin{bmatrix} 0_{2\times2} & 0_{2\times2} & 0_{2\times1} \\ 0_{2\times2} & rI_2 & 0_{2\times1} \\ 0_{1\times2} & 0_{1\times2} & \xi(x) \end{bmatrix} \tag{42}$$

With:

$$\xi(x) = \frac{T_{em}^* - T_{em}(x_e)}{\omega - \omega^*} \tag{43}$$

And:

$$T_{em}^* = C_f \omega^* \tag{44}$$

When substituted into the CL Hamiltonian equation, the term $\xi(x)$ is multiplied by $(\omega - \omega^*)$, which removes the singularity.
The formula for V_r in terms of $J_{rm}(x)$ is unaltered since only the mechanical portion of (34) has been altered.
By utilizing the equilibrium equations, we can ascertain:

$$J_{rm}(x) = MJ_2 I_s \tag{45}$$

The CL dynamic system consistently employs the formulation presented in equation (30), which comprises:

$$J_d(x) = \begin{bmatrix} -\omega_s L_s J_2 & -\omega_s M J_2 & 0_{2\times1} \\ -\omega_s L_s J_2 & -\omega_r L_s J_2 & MJ_2 I_s \\ 0_{1\times2} & MI_S^T J_2 & 0 \end{bmatrix};\ R_d(x) = \begin{bmatrix} R_s I_2 & 0_{2\times2} & 0_{2\times1} \\ 0_{2\times2} & (R_r + r)I_2 & 0_{2\times1} \\ 0_{1\times2} & 0_{1\times2} & T_f + \xi(x) \end{bmatrix} \tag{46}$$

Lastly, the rotor voltages of the control are expressed as follows:

$$V_r = V_r^* - (\omega - \omega^*)(L_r J_2 I_r^* + MJ_2 I_s) - M\omega^* J_2(I_s - I_s^*) - rI_2(I_r - I_r^*) \tag{47}$$

With:

$$V_r^* = (\omega_s - \omega^*)(L_r J_2 I_r^* + MJ_2 I_s^*) + R_r I_2 I_r^* \tag{48}$$

A Passivity-based control block diagram applied to a DIFG can be designed using Equations (47) and (48), as illustrated in Figure 4.

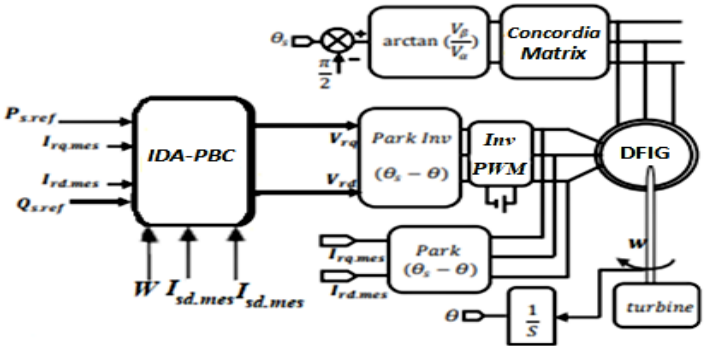

Fig. 4. Diagram of the Passivity-based control structure.

Journal of Information Systems Engineering and Management
2025, 10(4)
e-ISSN: 2468-4376
https://www.jisem-journal.com/

Research Article

Design of the Passivity-Fuzzy Logic Controller

Context of fuzzy logic sets

In 1965, Professor Zadeh introduced fuzzy set theory. This theory allows a degree of truth (membership) to be assigned to a variable that may be linguistic. This gradation of membership allows for the modeling of human observations expressed by IF-THEN linguistic rules [25]. However, Type 1 fuzzy logic systems (T1-FLS) have limitations when it comes to managing uncertainties and nonlinearities due to their distinct membership values. This led to the development of T2-FLS, which were first introduced by L. Zadeh. There have been recent advancements in the theoretical foundations of type 2 systems [12, 26]. The primary characteristic, the footprint of uncertainty (FOU), addresses these uncertainties and nonlinearities efficiently. Research indicates that type 2 systems are significantly more robust in the face of these challenges than type 1 systems [27, 28].

Combining IT2-FLC and IDA-PBC for the DFIG

The proposed framework uses a nested loop, in which the outer loop applies the IT2-FLC approach for energy management. The inner loop of the IDA-PBC is converted into a dynamic feedback system based on recorded states, such as rotor and stator currents and speed. The proposed controller is illustrated in Figure 5.

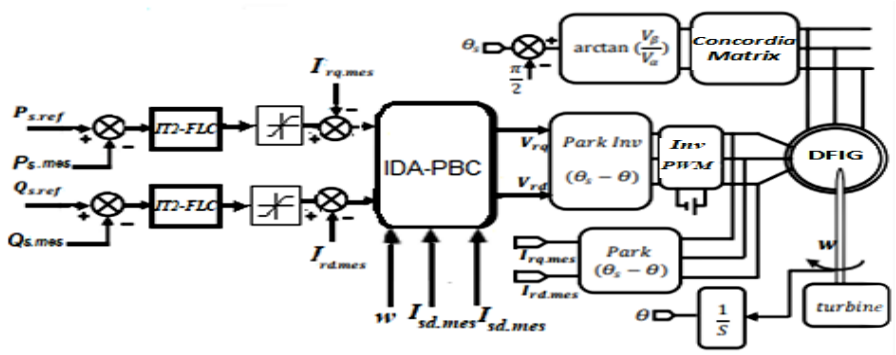

Fig.5. Diagram of Passivity-based Control using a fuzzy logic block.

Figure 6 illustrates the membership functions corresponding to the premises and consequences. The input and output discourse domains are scaled to the interval [-1, 1].

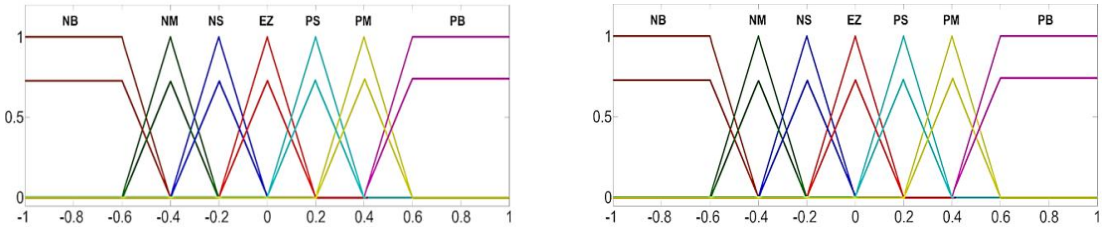

(a) *(b)*

Fig.6. (a) MF for inputs e and de, (b) MF for output

The aforementioned M rules can be represented by an inference matrix. Table 1 shows the fuzzy rules associated with the controller employed in this study.

Table 1. Rule table used by the T2-FLC

de / e	NB	NM	NS	ZE	PS	PM	PB
NB	NB	NB	NB	NB	NM	NS	ZE
NM	NB	NB	NB	NM	NS	ZE	PS
NS	NB	NB	NM	NS	ZE	PS	PM
ZE	NB	NM	NS	ZE	PS	PM	PB
PS	NM	NS	ZE	PS	PM	PB	PB
PM	NS	ZE	PS	PM	PB	PB	PB
PB	ZE	PS	PM	PB	PB	PB	PB

Journal of Information Systems Engineering and Management
2025, 10(4)
e-ISSN: 2468-4376
https://www.jisem-journal.com/

Research Article

Simulation Results

In this part of the simulation, a 10 kW generator is connected to a 400V/50 Hz network, with system parameters detailed in Table 2. The VC, SMC, IDA-PBC, and PFLC controllers are compared based on three criteria:

1) Operation at constant WS.
2) Operation at variable WS with optimized MPPT control.
3) Robustness evaluation against DFIG parameter variations.

Table 2: Parameters of the 10 kW wind conversion chain .

Parameters	Value	Parameters	Value
Rs (Stator resistance)	0.455 Ω	P (Number of pole pairs)	2
Rr (Rotor resistance)	019 Ω	ρ (Air density)	1.225Kg/m^3
Ls (Stator inductance)	0.07 H	R_b (Blade radius)	3.45m
Lr (Rotor inductance)	0.0213 H	H_m (Inertia constant)	2s
M (Mutual inductance)	0.034 H	D (Damping coefficients)	0.01Nm.s/rad

Fixed wind speed operation

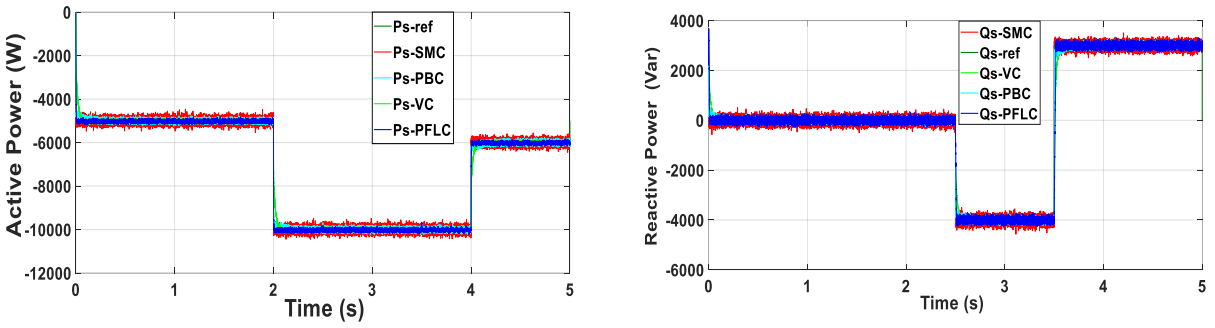

(a) *(b)*

Fig.7. Comparison of DFIG power: (a) Ps and (b) Qs under fixed wind speed conditions.

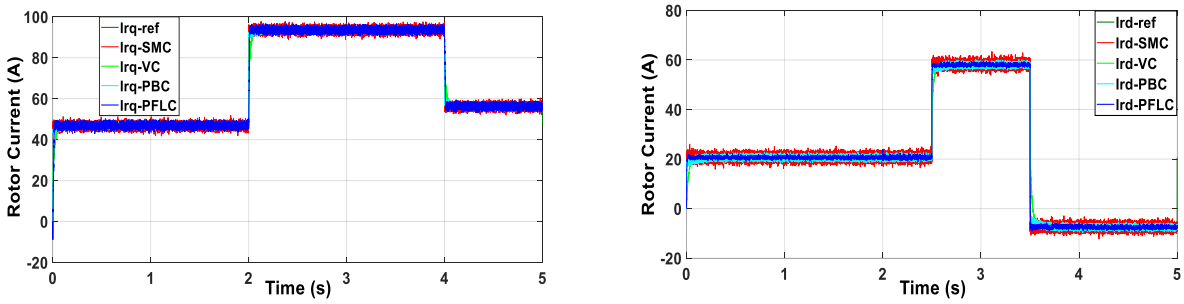

(a) *(b)*

Fig.8. Rotor current: (a) I_{rq} and (b) I_{rd}

The simulation results shown in Figure 7 demonstrate that the Passivity-Fuzzy Logic Control (PFLC), Passivity-based Control (PBC), sliding mode control (SMC), and vector control (VC) techniques can perfectly separate the two power components of the stator with excellent performance. In the setpoint tracking test, the controlled variables follow their reference trajectories precisely, maintaining active and reactive power within limits and achieving zero steady-state error. Furthermore, Figure 8 shows that the rotor currents on the d and q axes (I_{rd} and I_{rq}), which are associated with the stator's Qs and Ps respectively, have evolved in line with the reference trajectories with no overshoot.

Journal of Information Systems Engineering and Management
2025, 10(4)
e-ISSN: 2468-4376
https://www.jisem-journal.com/

Research Article

Operation at variable wind speed with optimized MPPT control

In this test, the wind turbine operates under variable WS, with an average velocity of 10 m/s. The MPPT strategy is used to produce Ps, while Qs is maintained at zero to keep the DFIG stator's power factor at unity.

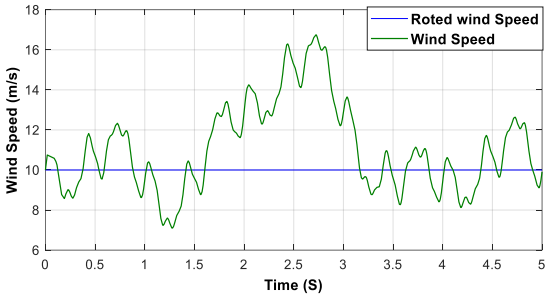

Fig.9. Wind speed (V) profile

Figure 9 illustrates a wind velocity of about 10 m/s. Below the nominal speed, the WT functions in MPPT mode, generating optimal power output. When wind speed exceeds the nominal amount, the controller modifies turbine rotation to maintain a consistent power output between 1.7 s and 3.2 s. Power output is highly sensitive to wind speed due to its cubic relationship. The negative value of Ps indicates that the DFIG is actively producing electrical power and feeding it into the grid. Qs was reduced to zero to maintain a consistent power factor, as depicted in Figure 10(b). The PFLC, IDA-PBC, SMC, and VC controllers exhibited commendable performance, particularly the PFLC, which demonstrated exceptional transient response and rapid convergence to reference objectives. These solutions accomplished flawless decoupling of the two stator power components. Ripples were also observed at the Ps and Qs levels, with these ripples being larger in the case of SMC and smaller in the case of PFLC compared to the other commands.

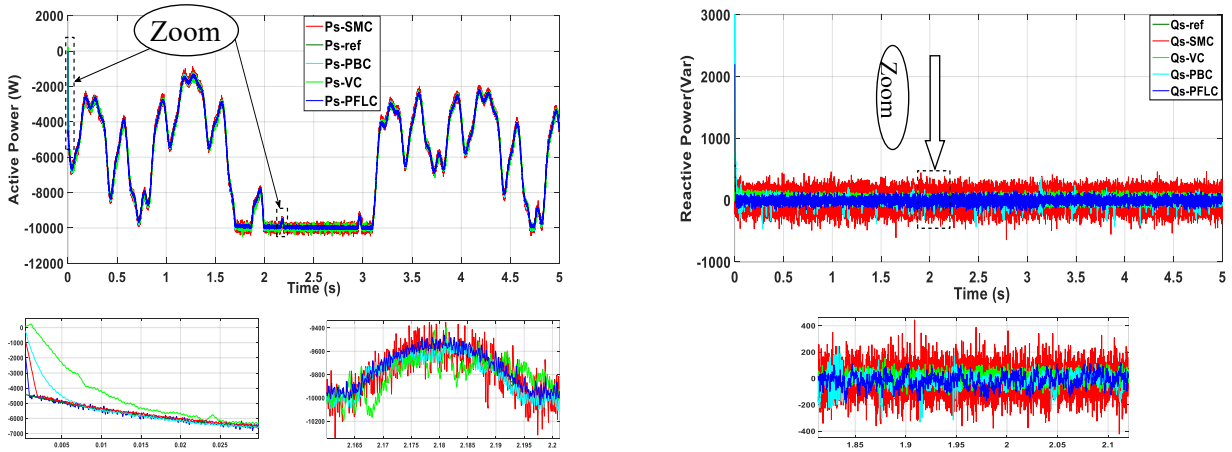

(a) *(b)*

Fig.10. Comparison of DFIG power: (a) Ps and (b) Qs under variable wind speed conditions.

Robustness Evaluation against DFIG Parameter Variations

After confirming good setpoint tracking, we evaluate the system's robustness against parameter uncertainty by doubling R_s and R_r, decreasing L_s and L_r by 30%, and reducing M to half of its nominal value.

Journal of Information Systems Engineering and Management
2025, 10(4)
e-ISSN: 2468-4376
https://www.jisem-journal.com/

Research Article

Qualitative Comparison of Robustness

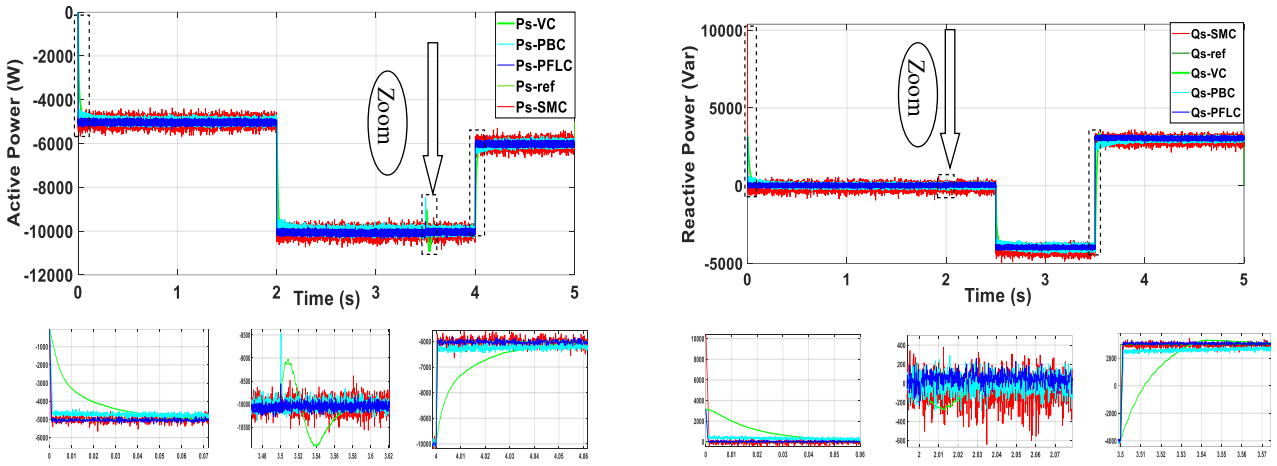

(a) *(b)*

Fig.11. Comparison of DFIG power: (a) Ps and (b) Qs under parameter variations.

Figure 11 compares four controllers tested for effectiveness and robustness against parametric uncertainties and disturbances. The vector control (VC) and Passivity-based control (PBC) showed minor overshoot briefly before tracking the reference signal. In contrast, the passivity-fuzzy logic controller (PFLC) and sliding mode control (SMC) had no overshoot and were precise. The PFLC was the most efficient and effective, offering a faster response, quicker damping of small overshoots, and better adaptation to changing setpoints. Next was the SMC, followed by the PBC and lastly the VC. The PFLC reduced Qs and Ps ripples more than the other controllers.

Quantitative Robustness Comparison

This assessment is founded on three static error criteria e (Ps and Qs): integrated squared error (ISE), integral absolute error (IAE), and the time-weighted integral of the absolute error (ITAE). These metrics are employed to assess the performance of the four controllers and are mathematically defined as follows [29]:

$$\text{ISE}=\int_0^T e^2(t)dt \tag{49}$$

$$\text{IAE}=\int_0^T |e(t)|dt \tag{50}$$

$$\text{ITAE}=\int_0^T t|e(t)|dt \tag{51}$$

To calculate these three criteria, the commands and errors of the controlled variables were used. These calculations were performed over a 5 s simulation period, employing power setpoints consistent with those defined in the simulation conditions. A quantitative comparison of robustness is presented in Table 3.

Table 3. Quantitative comparative study based on the time and error between the developed commands.

	Criterion	Commands Developed			
		Vector Control	passivity-based Control	Sliding Mode Control	Passivity-Fuzzy Logic Control
Active power	$\text{ISE}=\int_0^T e^2(t)dt$	492.2	427.2	418.6	292.3
	$\text{IAE}=\int_0^T \|e(t)\|dt$	1158	1062	1033	637.6
	$\text{ITAE}=\int_0^T t\|e(t)\|dt$	$2.825e^5$	$2.771\ e^5$	$2.712\ e^5$	$2.635\ e^5$
Reactive power	$\text{ISE}=\int_0^T e^2(t)dt$	453.2	447.5	436.7	337.3
	$\text{IAE}=\int_0^T \|e(t)\|dt$	1097	1085	1072	801.2
	$\text{ITAE}=\int_0^T t\|e(t)\|dt$	$3.591e^5$	$3.396\ e^5$	$3.226\ e^5$	$2.928\ e^5$

Research Article

This comparison evaluates the differences in simulation outcomes resulting from variations in generator parameters, thus highlighting the effectiveness of each control method in calculating ISE, IAE and ITAE. The results in Table 3 reveal that passivity-fuzzy logic control performs best in minimizing the ISE, IAE and ITAE criteria during parameter changes, followed by sliding mode control, Passivity-based Control and finally vector control.

CONCLUSION

This paper presented a comparative analysis of four control strategies—VC, SMC, IDA-PBC, and PFLC for regulating active and reactive power in a DFIG-based WECS. While all methods demonstrated good tracking and stability under nominal conditions, the PFLC showed superior performance in terms of response time, robustness to parameter variations, and disturbance rejection.

Simulation results confirmed that integrating interval type-2 fuzzy logic with passivity-based control improves power quality and minimizes steady-state error and overshoot. Quantitative metrics further highlighted the PFLC as the most effective solution among the tested techniques.

These findings suggest that PFLC is a promising approach for advanced wind turbine control, offering both high efficiency and enhanced reliability. Future work will focus on experimental validation and further optimization to ensure readiness for practical deployment in modern renewable energy systems.

REFERENCES

[1] Xiong, L., Li, J., Li, P., Huang, S., Wang, Z., & Wang, J. Event triggered prescribed time convergence sliding mode control of DFIG with disturbance rejection capability, International Journal of Electrical Power & Energy Systems, vol. 131 pp. 106970, 2021. https://doi.org/10.1016/j.ijepes.2021.106970.

[2] Mousavi, Y., Bevan, G., Kucukdemiral, I. B., & Fekih, A., Sliding mode control of wind energy conversion systems: Trends and applications, Renewable and Sustainable Energy Reviews, 167 ,pp. 112734, 2022. https://doi.org/10.1016/j.rser.2022.112734

[3] GWEC. Global Wind Report 2024. Global Wind Energy Council, 2024.

[4] Benbouhenni, H., Bizon, N., Mosaad, M. I., Colak, I., Djilali, A. B., & Gasmi, H, Enhancement of the power quality of DFIG-based dual-rotor wind turbine systems using fractional order fuzzy controller, Expert Systems with Applications, 238 ,pp. 121695, 2024. https://doi.org/10.1016/j.eswa.2023.121695

[5] Khan, D., Ahmed Ansari, J., Aziz Khan, S., & Abrar, U." Power optimization control scheme for doubly fed induction generator used in wind turbine generators". Inventions, 5(3) ,pp. 40, 2020. https://doi.org/10.3390/inventions5030040

[6] Kaloi, G. S., Baloch, M. H., Kumar, M., Soomro, D. M., Chauhdary, S. T., Memon, A. A., & Ishak, D., An LVRT scheme for grid-connected DFIG based WECS using state feedback linearization control technique, Electronics, 8(7) ,pp. 777, 2019. https://doi.org/10.3390/electronics8070777

[7] Marques, G.D., Iacchetti, M.F., DFIG Topologies for DC Networks: A Review on Control and Design Features. IEEE Trans. Power Electr, 34(2) ,pp.1299–1316, 2019.https://doi: 10.1109/TPEL.2018.2829546

[8] Mousavi, Y., Bevan, G., Kucukdemiral, I. B., & Fekih, A., Sliding mode control of wind energy conversion systems: Trends and applications, Renewable and Sustainable Energy Reviews 167 , pp 112734, 2022. https://doi.org/10.1016/j.rser.2022.112734

[9] Amira, L., Tahar, B., & Abdelkrim, M, Sliding mode control of doubly-fed induction generator in wind energy conversion system. In: 2020 8th International Conference on Smart Grid (icSmartGrid). IEEE,. pp. 96-100, 2020. https://doi: 10.1109/icSmartGrid49881.2020.9144778

[10] Mancini, M., E. Capello, and E. Punta, Sliding mode control with chattering attenuation and hardware constraints in spacecraft applications, IFAC-PapersOnLine 53(2) , pp. 5147-5152, 2020. https://doi.org/10.1016/j.ifacol.2020.12.1174

[11] Nicklasson, P. J., Ortega, R., Espinosa-Perez, G., & Jacobi, C. G. J. Passivity-based control of a class of Blondel-Park transformable electric machines. IEEE Transactions on Automatic Control, 42(5) , pp 629-647,2002. https://doi: 10.1109/9.580867

[12] Hassani, H., & Zarei, J., Interval Type-2 fuzzy logic controller design for the speed control of DC motors. Systems Science & Control Engineering, 3(1) , pp. 266-273, 2015. https://doi: 10.1080/21642583.2015.1013644

[13] Belkhier, Y., Achour, A., Bures, M., Ullah, N., Bajaj, M., Zawbaa, H. M., & Kamel, S, Interconnection and damping assignment passivity-based non-linear observer control for efficiency maximization of permanent magnet synchronous motor, Energy Reports, 8 , pp. 1350-1361, 2022. https://doi.org/10.1016/j.egyr.2021.12.057

[14] Sahri, Y., Tamalouzt, S., Lalouni Belaid, S., Bacha, S., Ullah, N., Ahamdi, A. A. A., & Alzaed, A. N, Advanced fuzzy 12 dtc control of doubly fed induction generator for optimal power extraction in wind turbine system under random wind conditions, *Sustainability*, 13(21) ,pp 11593, 2021. https://doi.org/10.3390/su132111593

[15] Adeyanju, A. A. The Influence Of Rotor Separation On The Performance Of A Dual-Rotor Wind Turbine, Journal of Namibian Studies, *History Politics Culture*, 35,pp 4684-4702, 2023. https://doi: https://doi.org/10.59670/jns.v35i.4573

[16] Shuaibu, M., Abubakar, A. S., & Shehu, A. F, Techniques for ensuring fault ride-through capability of grid connected DFIG-based wind turbine systems: a review, Nigerian Journal of Technological Development, 18(1) ,pp 39-46, 2021. http://dx.doi.org/10.4314/njtd.v18i1.6

[17] Carpintero-Renteria, M., Santos-Martin, D., Lent, A., & Ramos, C, Wind turbine power coefficient models based on neural networks and polynomial fitting., IET Renewable Power Generation, 14(11) ,pp. 1841-1849, 2020. https://doi.org/10.1049/iet-rpg.2019.1162

[18] Castillo, OC, Andrade, VR, Rivas, JJR, & González, RO., Comparison of power coefficients in wind turbines considering the tip speed ratio and blade pitch angle., *Energies* , 16(6) ,pp2774, 2023. https://doi.org/10.3390/en16062774

[19] Hemeyine, A. V., Abbou, A., Tidjani, N., Mokhlis, M., & Bakouri, A., Robust Takagi Sugeno fuzzy models control for a variable speed wind turbine based on a DFIG, International Journal of Intelligent Engineering and Systems, 13(3) ,pp90-100, 2020. https://doi: 10.22266/ijies2020.0630.09

[20] Mousa, H. H., Youssef, A. R., & Mohamed, E. E., Hybrid and adaptive sectors P&O MPPT algorithm based wind generation system. *Renewable Energy*, 145,pp.1412-1429, 2020. https://doi.org/10.1016/j.renene.2019.06.078

[21] Kadri, A., Marzougui, H., Aouiti, A., & Bacha, F., Energy management and control strategy for a DFIG wind turbine/fuel cell hybrid system with super capacitor storage system, Energy, 192,pp 116518, 2020. https://doi.org/10.1016/j.energy.2019.116518

[22] Chakib, M., Nasser, T., & Essadki, A., Comparative study of active disturbance rejection control with RST control for variable wind speed turbine based on doubly fed induction generator connected to the grid. International Journal of Intelligent Engineering and Systems, 13(1) ,pp.248-258, 2020. https://doi: 10.22266/ijies2020.0229.23

[23] V. Utkin, «Sliding Modes in Control and Optimization». Berlin, Germany: Springer-Verlag, 1992 https://doi: lO.1007/978-3-642-84379-2

[24] Slotine, J. J. E., & Li, W, *Applied nonlinear control*. Englewood Cliffs, NJ: Prentice hall. 199(1) , p. 705, 1991.

[25] Saidi, A., Naceri, F., Youb, L., Cernat, M., & Pesquer, L. G. Two types of fuzzy logic controllers for the speed control of the doubly-fed induction machine. Advances in Electrical and Computer Engineering, 20(3) , pp. 65-74, 2020. https://doi .10.4316/AECE.2020.03008

[26] Acikgoz, H., Kececioglu, O., Gani, A., Tekin, M., & Sekkeli, M., Robust control of shunt active power filter using interval type-2 fuzzy logic controller for power quality improvement, Tehnicki Vjesnik-Technical Gazette, 24,pp.363-368, 2017. https://doi.org/10.17559/TV-20161213004749

[27] Yan, S. R., Dai, Y., Shakibjoo, A. D., Zhu, L., Taghizadeh, S, Ghaderpour, E., & Mohammadzadeh, A A fractional-order multiple-model type-2 fuzzy control for interconnected power systems incorporating renewable energies and demand response, Energy Reports, 12 ,pp. 187-196, 2024. https://doi.org/10.1016/j.egyr.2024.06.018

[28] I. Allali, B.Dehiba, A Comparative Study of Interval Type-2 and Type-1 Fuzzy Sliding Mode in Controlling DFIG-Based Wind Energy Conversion System, Nigerian Journal Of Technological Development,22(3) , pp 101-110, 2025. https://doi.org/10.63746/njtd.v22i3.2818

[29] Herizi, A., & Rouabhi, R. Hybrid Control Using Sliding Mode Control with Interval Type-2 Fuzzy Controller of a Doubly Fed Induction Generator for Wind Energy Conversion. International Journal of Intelligent Engineering & Systems, 15(1) ,pp 549-562, 2022. https://doi: 10.22266/ijies2022.0228.50